

UC San Diego

UC San Diego Previously Published Works

Title

Yet more evidence that myelin protons can be directly imaged with UTE sequences on a clinical 3T scanner: Bicomponent analysis of native and deuterated ovine brain specimens

Permalink

<https://escholarship.org/uc/item/66m2j2fx>

Journal

Magnetic Resonance in Medicine, 80(2)

ISSN

0740-3194

Authors

Fan, Shu-Juan
Ma, Yajun
Zhu, Yanchun
[et al.](#)

Publication Date


2018-08-01

DOI

10.1002/mrm.27052

Peer reviewed

Yet More Evidence That Myelin Protons Can Be Directly Imaged With UTE Sequences on a Clinical 3T Scanner: Bicomponent T_2^* Analysis of Native and Deuterated Ovine Brain Specimens

Shu-Juan Fan , Yajun Ma, Yanchun Zhu, Adam Searleman, Nikolaus M. Szeverenyi, Graeme M. Bydder, and Jiang Du*

Purpose: UTE sequences with a minimal nominal TE of $8\mu\text{s}$ have shown promise for direct imaging of myelin protons ($T_2 < 1\text{ ms}$). However, there is still debate about the efficiency of 2D slice-selective UTE sequences in exciting myelin protons because the half excitation pulses used in these sequences have a relatively long duration (e.g., 0.3–0.6 ms). Here, we compared UTE and inversion-recovery (IR) UTE sequences used with either hard or half excitation pulses (durations $32\mu\text{s}$ or $472\mu\text{s}$, respectively) for imaging myelin in native and deuterated ovine brain at 3T.

Methods: Freshly frozen ovine brains were dissected into $\sim 2\text{ mm}$ -thick pure white matter and ~ 3 to 8 mm -thick cerebral hemisphere specimens, which were imaged before and/or after different immersion time in deuterium oxide.

Results: Bicomponent T_2^* analysis of UTE signals obtained with hard excitation pulses detected an ultrashort T_2 component (STC) fraction (f_S) of 0% to 10% in native specimens, and up to $\sim 86\%$ in heavily deuterated specimens. f_S values were significantly affected by the TIs used in IR-UTE sequences with either hard or half excitation pulses in native specimens but not in heavily deuterated specimens. The STC T_2^* was in the range of 150 to $400\mu\text{s}$ in all UTE and IR-UTE measurements obtained with either hard or half excitation pulses.

Conclusion: Our results further support myelin protons as the major source of the ultrashort T_2^* signals seen on IR-UTE images and demonstrate the potential of IR-UTE sequences with half excitation pulses for directly imaging myelin using clinical scanners. *Magn Reson Med* 80:538–547, 2017. © 2017 International Society for Magnetic Resonance in Medicine.

Key words: T_2^* ; bicomponent; myelin; white matter; UTE; inversion recovery

INTRODUCTION

Conventional imaging of brain tissue commonly detects three distinct pools: a long T_2 pool associated with free

water in cerebrospinal fluid (T_2 , $\sim 2\text{ s}$), an intermediate T_2 pool involving extra- and intracellular water (T_2 , $\sim 100\text{ ms}$), and a short T_2 pool composed of water trapped in myelin bilayers and other associated macromolecules (myelin water) (T_2 , 1–10 ms) (1,2). Studying free water signals is helpful for detecting increased permeability of the blood–brain barrier in stroke and other pathological conditions (3–5). Characterizing extra- and intracellular water signals have been useful for probing not only cellular structural characteristics but also functional activation (6–9). Investigating myelin water indirectly provides insights about the integrity of myelin and myelin loss (10–12). These water protons can be characterized using currently available clinical MRI techniques with TEs of 1 ms and longer, and are referred to as *long T_2 components* (LTCs) in this study.

Unlike most water protons, the semisolid highly constrained lipid protons trapped in myelin sheaths, named as *myelin protons* hereafter (13), have ultrashort T_2 ($< 1\text{ ms}$) and are not directly detectable with most conventional MRI sequences (14). Direct imaging of myelin protons may improve the specificity of MRI for evaluation of neurological diseases characterized by demyelination and remyelination, such as multiple sclerosis (15,16), and may also be of value in monitoring therapeutic response. In recently developed 2D UTE sequences, nominal TEs as short as $8\mu\text{s}$ can be achieved through half pulse excitation, variable rate selective excitation, radial ramp sampling, and fast transmit/receive switching (17,18), making it possible to directly image myelin protons. Furthermore, inversion-recovery (IR) UTE sequences can provide robust suppression of signals from LTCs using an adiabatic IR preparation pulse and therefore have the potential to directly and selectively image myelin with high contrast (19).

Although UTE imaging of myelin protons has been investigated by several groups (14,18,20–23), there is still debate about whether UTE sequences, especially when used with half excitation pulses (for which the pulse duration is on the order of hundreds of microseconds), can directly detect myelin proton signals that have a reported T_2^* of $\sim 300\mu\text{s}$ (22) or shorter (14,21). This study aimed to compare UTE and IR-UTE sequences used with either short hard or longer half excitation pulses for probing myelin proton signals at 3T, and meanwhile to probe the specificity and sensitivity of these sequences to myelin proton signals by comparing the ultrashort T_2

Department of Radiology, University of California, San Diego, California, USA.

Grant sponsor: National Institute of Neurological Disorders and Stroke, National Institutes of Health (NINDS, NIH); Grant number: R01NS092650.

*Correspondence to: Jiang Du, University of California, San Diego, Department of Radiology, 200 West Arbor Drive, San Diego, CA 92103-8756, USA. E-mail: jiangdu@ucsd.edu

Received 21 July 2017; revised 5 November 2017; accepted 29 November 2017

DOI 10.1002/mrm.27052

Published online 21 December 2017 in Wiley Online Library (wileyonlinelibrary.com).

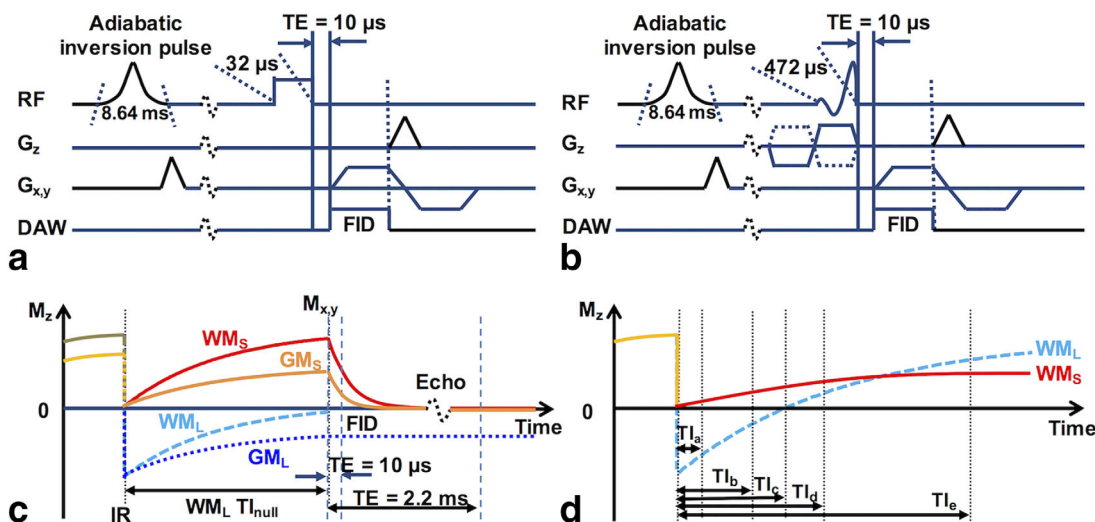


FIG. 1. Diagrams of the 2D IR-UTE pulse sequences with TE of 10 μs used with (A) a short hard-excitation pulse (rectangular shape, duration 32 μs, bandwidth=8.2 kHz) followed by 2D radial ramp sampling, and (B) a half excitation pulse (duration 472 μs, bandwidth=2.7 kHz) followed by 2D radial ramp sampling. (C) Illustration of the contrast mechanism for imaging white-matter ultrashort T₂ components (WM_S) using IR-UTE with the TI set for nulling of signals from the white-matter long T₂ components (WM_L), with the TI termed as WM_L TI_{null}. In magnitude IR-UTE images, the signal in white matter quickly decays to zero with increasing TE, whereas the signal in gray matter is still high at TE = 2.2 ms because it is dominated by long T₂ components (GM_L). (D) M_z of WM_L and WM_S plotted against different TIs at the time UTE acquisition starts. At T_{Ic}, signals from WM_L are nulled. At T_{Ib}, which is much shorter than T_{Ic}, signal in the white matter is dominated by WM_L. At T_{Ib}, which is only slightly shorter than T_{Ic}, signal from WM_S is cancelled out by that from WM_L. At T_{Id} and T_{If}, signals from WM_S and WM_L coexist in the image but with different fractions. Note that the time parameters in the diagrams were not proportionally illustrated. IR, inversion recovery; GM, gray matter; WM, white matter.

component (STC) fraction (f_s) and T_2^* (T_{2S}^*) seen in fresh and deuterated ovine brain white matter (WM). Deuterons in deuterium oxide (D₂O) have a MR frequency ~6.5 times lower than that of protons and are not detectable with proton MRI (24). By immersing tissue specimens in highly purified D₂O, it is possible to replace the majority, if not all, of the long T₂ water protons with deuterons (14). The specimens were expected to have different proportions of ¹H MRI-visible LTCs after they were immersed in D₂O for different durations, whereas myelin protons would survive the D₂O exchange (14) and still be detectable with UTE and IR-UTE sequences. If myelin protons are the major source of the ultrashort T₂ signals and the sequences are sensitive to proportional changes of these signals, T_{2S}^* might not change; however, f_s would change significantly after the exchange.

METHODS

Pulse Sequences and Contrast Mechanisms

Figure 1 shows diagrams of the 2D IR-UTE pulse sequences and the associated contrast mechanisms. Either a short hard pulse (rectangular shape, duration 32 μs, bandwidth=8.2 kHz) or a half pulse (half-sinc shape, variable rate selective excitation-corrected, duration 472 μs, bandwidth=2.7 kHz) was used for signal excitation (Figs. 1A–1B). Each sequence contained an adiabatic IR preparation pulse (Silver–Hoult pulse, duration 8.64 ms, bandwidth=1.4 kHz) and a minimal nominal TE of 10 μs. The basis for contrast seen on the IR-UTE images for selective myelin proton imaging in WM is illustrated

in Figures 1C and 1D. The inversion time (TI) is chosen to null the signals from LTCs in WM (WM_L, and this TI is abbreviated as WM_L TI_{null} in this paper). At the time the UTE acquisition starts (TE = 10 μs), LTCs in gray matter (GM_L) have nonzero negative magnetization (because GM_L has a longer T₁ than WM_L), whereas STCs in WM and GM (i.e., WM_S and GM_S) have nonzero-positive magnetizations (Fig. 1C). Therefore, on the IR-UTE images obtained at WM_L TI_{null} and TE = 10 μs, the WM signal comes from STCs, whereas the GM signal contains mixed contributions from both LTCs and STCs. When the selected TI is incrementally offset from WM_L TI_{null}, WM signals in the image will be increasingly contaminated by LTCs, leading to inaccurate measurement of STC signals (presumably mainly from myelin protons) (Fig. 1D). WM_L TI_{null} can be estimated from IR-UTE images obtained with varying TIs at a later yet still short TE (e.g., TE = 2.2 ms). At this TE, the magnetization of STCs is zero or near zero due to fast signal decay, whereas that of LTCs is largely unchanged, allowing selective measurement of the signals from LTCs for the estimation of their T₁ and TI_{null}.

Hard excitation pulses have higher power and shorter duration than half excitation pulses, and thus should be more efficient and reliable in exciting extremely short T₂ protons (25). However, a half pulse has to be used for 2D slice-selective imaging. In this study, the slice-selective gradients were turned off in the half pulse excitation experiments based on the following three considerations: First, the specimens were carefully prepared into pure WM specimens (~2 mm thick) or thin coronal hemisphere slabs (~3–8 mm thick); thus, a region of interest (ROI)

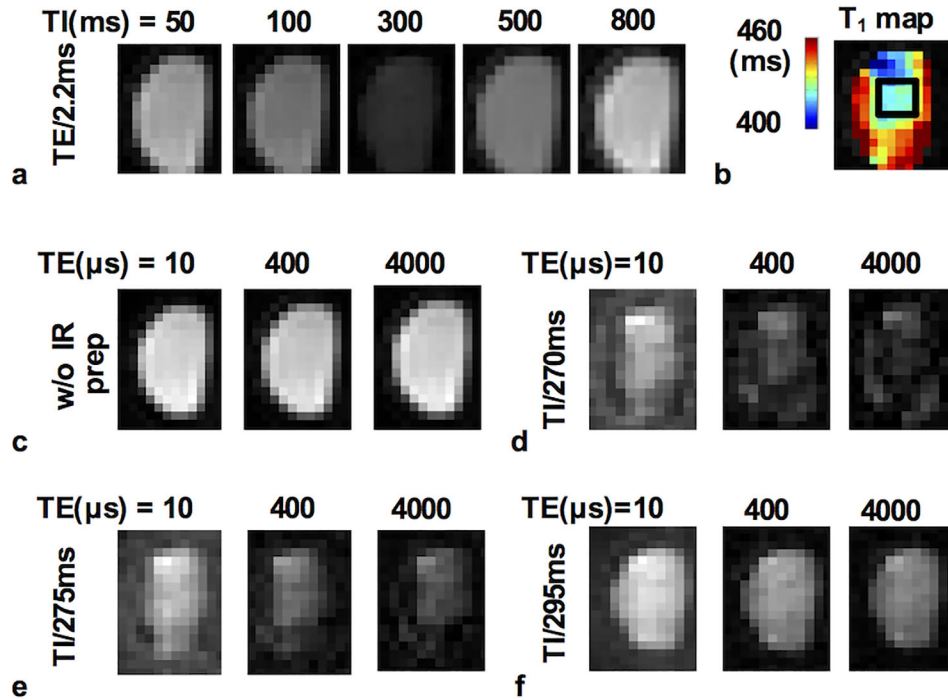


FIG. 2. Representative magnitude images (acquired with hard excitation pulses) of one native white-matter short block. (A) Images obtained with varying TIs at TE=2.2 ms. (B) T₁ map calculated from the images in (A) showing a relatively homogeneous center and a rim with a slightly longer T₁. The black box shows the region of interest used for quantitative T₂^{*} analyses. (C) Images obtained with different TEs w/o IR prep. (D–F) Images obtained with different TEs and varying TIs. There was an obvious signal intensity decrease with the increase of TE in the images at TIs=270 ms and 275 ms but not at TI=295 ms. IR, inversion recovery; w/o IR prep, without inversion recovery preparation.

could be defined in WM without contamination from neighboring GM when the specimen was excited without slice selection. Second, errors induced by eddy currents in regular half pulse excitation experiments could be eliminated by turning off the slice-selective gradients, thus providing more accurate estimations of T_{2S}^{*} and f_S, as well

as allowing a more direct comparison between the hard pulse and half pulse excitations. Third, regular 2D UTE and IR-UTE imaging using half excitation pulses would require two excitations per scan to achieve slice selection. The total scan time could therefore be halved by turning off the slice-selective gradients.

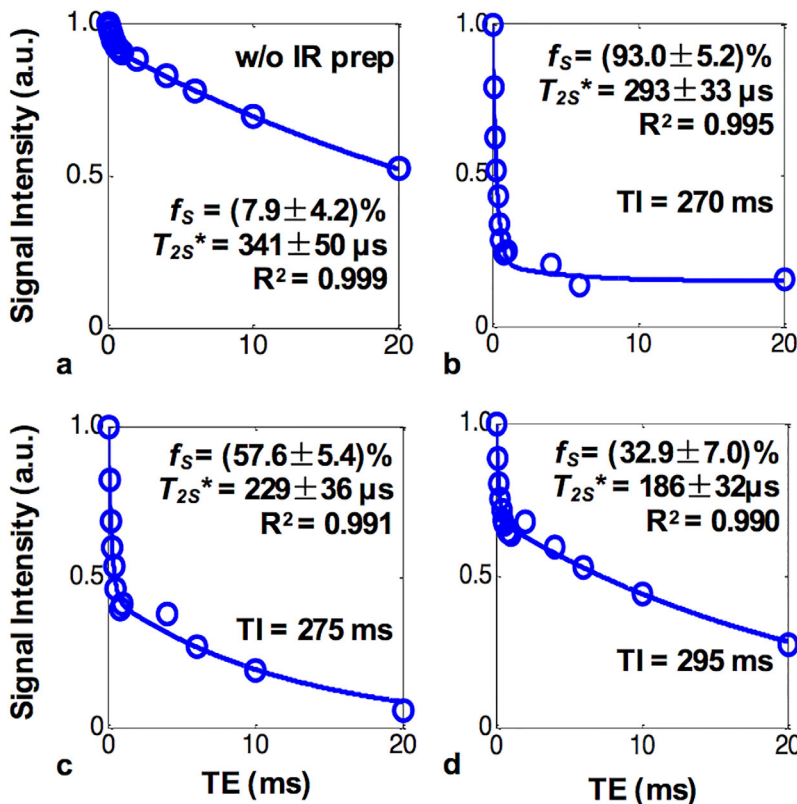


FIG. 3. Representative bicomponent T₂^{*} fitting curves of one native white-matter short block. (A) Measurement with hard excitation pulses and no inversion-recovery preparation. (B–D) Measurements with hard excitation pulses and varying TIs. All measurements provided different f_S but similar T_{2S}^{*} values. f_S, ultrashort T₂ component fraction; T_{2S}^{*}, ultrashort T₂ component T₂^{*}; w/o IR prep, without inversion recovery preparation.

Specimen Preparation and Experimental Design

Five freshly frozen ovine brains were thawed and dissected into six ~ 2 mm-thick $\sim 2 \times 5$ mm² pure WM short blocks, three ~ 2 mm-thick $\sim 4 \times 10$ mm² pure WM long segments from three consecutive slabs of the same brain, one ~ 8 mm-thick cerebral hemisphere slab, and three ~ 3 mm-thick cerebral hemisphere slabs. Two WM short blocks, all three WM long segments, and all three ~ 3 mm-thick cerebral hemisphere slabs were subject to D₂O exchange. Each WM short block was immersed in 5 mL D₂O (99.9%, Sigma-Aldrich, St. Louis, Missouri) for 8 h with D₂O refreshed four times (8 h five-pass D₂O exchange). Each WM long segment was immersed in 5 mL D₂O for 1 h, 2 h (two 1 h consecutive periods with D₂O refreshed once), or 27 h (1 h, 1 h, 2 h, and 23 h consecutive periods with D₂O refreshed three times, that is, 27 h four-pass D₂O exchange), respectively. Each cerebral hemisphere slab was immersed in 10 mL D₂O and subject to 27 h four-pass D₂O exchange.

All of the pure WM short blocks were imaged using a 5 mm-diameter transmit/receive solenoid coil to achieve high signal-to-noise ratio (SNR). All the pure WM long segments and cerebral hemisphere slabs were imaged with a 7.6-cm receive-only surface coil that can be used clinically. First, three native WM short blocks were imaged with UTE sequences and IR-UTE sequences with varying TIs using hard excitation pulses. Then one deuterated WM short block was imaged with the UTE sequence using hard excitation pulse; and one native and one deuterated WM short block were each subject to free induction decay (FID) acquisition to evaluate water signal loss after D₂O exchange. Next, the ~ 8 mm-thick cerebral hemisphere slab was imaged in the native condition with UTE and IR-UTE sequences using both hard and half excitation pulses. Lastly, the three WM long segments were imaged after progressive D₂O exchange, and the three ~ 3 mm-thick cerebral hemisphere slabs were all imaged before and after 27 h D₂O exchange with UTE and IR-UTE sequences using half excitation pulses.

Data Acquisition

Both single-slice 2D UTE and IR-UTE sequences were implemented on a 3T Signa TwinSpeed scanner (GE Healthcare Technologies, Milwaukee, Wisconsin), which had a maximum gradient strength of 40 mT/m and a maximum slew rate of 150 mT/m/ms. The UTE sequence was performed with TR = 1,000 ms and a series of TEs ranging from 10 μ s to up to 30 ms. At each imaging time point, the IR-UTE sequence was first used with TR/TE = 1,000/2.2 ms and a series of TIs (50, 100, 300, 500, and 800 ms) to measure the WM_L T₁ and determine WM_L TI_{null}. The same IR-UTE sequence was then used with TR = 1,000 ms, TI = WM_L TI_{null} and/or TIs of 5 to 130 ms longer than WM_L TI_{null}, and a series of TEs ranging from 10 μ s to 30 ms to measure f_S and T_{2S}^* in WM. The acquisition matrix was 96 \times 96, and the scan time was 97s per acquisition. T₂-weighted multislice fast spin echo images were acquired with TR/TE = 3,000/40 ms, slice thickness = 1 mm, and no slice gap to guide the ROI definition in WM on the UTE and IR-UTE images. FID signals were acquired on an 11.7T small bore preclinical scanner (Bruker BioSpec 117/11 USR/R, Rheinstetten, Germany). Briefly, the specimen was

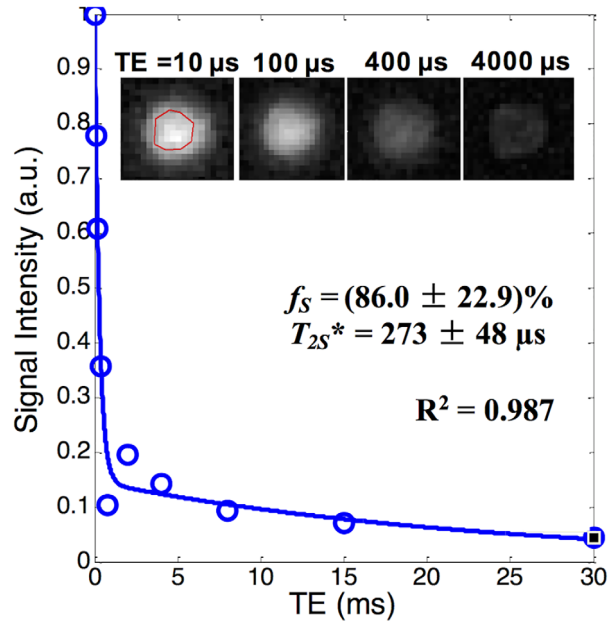


FIG. 4. Bicomponent T_2^* analysis of images acquired with hard excitation pulse and no inversion recovery preparation from a WM short block after a 27 h four-pass D₂O exchange, showing a much higher f_S with similar T_{2S}^* compared with a native WM short block as shown in Figure 3A. Inserts are the images of the WM short block after 27 h D₂O exchange, which showed fast signal decay with the increase in TE. WM, white matter; D₂O, deuterium oxide; f_S , ultrashort T₂ component fraction; T_{2S}^* , ultrashort T₂ component T₂.

placed inside a 5-mm NMR proton-free tube and examined using a custom-made proton-free coil with a block excitation pulse (pulse width = 20 μ s), TR = 20 s, 4,096 points, and sweep bandwidth = 50 kHz.

Data Analysis

The WM_L T₁ and TI_{null} were calculated offline in each manually defined ROI using a single-component three-parameter fitting model in MatLab (MathWorks, Natick, Massachusetts). T_{2S}^* and f_S were calculated using a previously published bicomponent fitting model in MatLab (MathWorks) (26):

$$S(TE) = A_S \times e^{-\frac{TE}{T_{2S}^*}} + A_L \times e^{-\frac{TE}{T_{2L}^*}} + noise, \quad [1]$$

where $S(TE)$ is the UTE or IR-UTE MR signal; A_S and A_L are the signal amplitudes of the STCs and LTCs; T_{2S}^* is the STC T₂^{*}; and T_{2L}^* is the LTC T₂^{*}. f_S was defined as $A_S/(A_S + A_L)$. Initially, all datasets were to bicomponent fitting. However, in some cases with exceptionally high fractions of LTCs or STCs, the two components were not clearly separated (i.e., both T₂^{*} values < 1 ms or both > 20 ms) using Equation [1]. Thus, to improve algorithmic stability, these cases were reanalyzed using a single-component fitting model:

$$S(TE) = S_0 \times e^{-TE/T_2^*} + noise, \quad [2]$$

where S_0 is the signal intensity at the minimum TE. The key fitting parameters are provided in the online

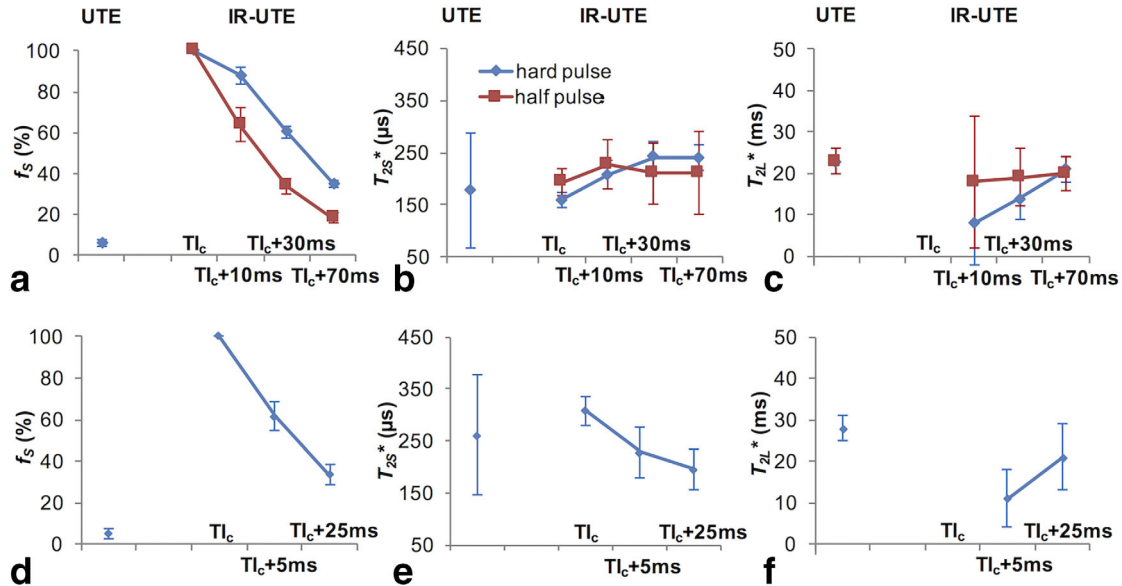


FIG. 5. T_2^* fitting results from the ~ 8 -mm-thick hemisphere slab imaged using both hard and half excitation pulse sequences (A–C) and the average results from three pure WM short blocks imaged using hard excitation pulse sequence (D–F). IR-UTE images were acquired with $TI = WM_L TI_{null}$ (labeled as TI_c , equivalent to that in Fig. 1D, on the x-axes of the figures) and 5 to 70 ms longer. The ultrashort T_2 component fraction (f_S) was very low when measured with UTE ($< 10\%$), much higher when measured with IR-UTE at $WM_L TI_{null}$, and decreased as TI increased from $WM_L TI_{null}$. The UTE sequence used with half pulse excitation did not detect the ultrashort T_2 component in this native specimen. f_S was consistently lower when measured with half pulse excitation than with hard pulse excitation at various TI s greater than $WM_L TI_{null}$ (A and D). The ultrashort T_2 component T_{2S}^* values were all in the range of 150 to 250 μs (B and E), and the long T_2 component T_2^* (T_{2L}^*) changed significantly with the increase in TI when hard pulse excitation was used (C and F). At $WM_L TI_{null}$, the T_2^* signal followed a single-component decay ($R^2 > 0.99$) (F). These results demonstrated the efficiency of the half-pulse UTE and IR-UTE sequences in measuring T_{2S}^* and detecting f_S changes in the presence of different proportions of signals from long T_2 components. WM, white matter; $WM_L TI_{null}$, inversion time for nulling signals from white-matter long T_2 components.

Supporting Information. All images used for analysis and presentation are magnitude images. Each FID was subject to Fourier transform as well as automatic phase and baseline corrections in iNMR (<http://www.inmr.net>) and displayed as a spectrum.

RESULTS

Figure 2 and Figure 3 show results from one native WM short block imaged using hard pulse excitation. Figure 2A shows obvious signal intensity variation in the magnitude images acquired with different TI s at $TE = 2.2$ ms, reflecting varying relative contributions from STCs and LTCs. The signal intensity was lowest at $TI = 300$ ms, suggesting significant suppression of the signals from LTCs (Fig. 2A). The T_1 map (Fig. 2B) calculated from the images in Figure 2A showed a near uniform structure inside the specimen, with marginal regions showing slightly longer T_1 s (the map scale was 400–460 ms), validating that the specimen was pure WM (T_1 of GM matter would be in the range of ~ 800 to 1,000 ms when measured using the same IR-UTE sequences (27)), although its margins might have been contaminated or injured during handling. Figure 2C shows magnitude images acquired with different TE s and no IR preparation. Figures 2D through 2F show magnitude images acquired with different TE s and varying TI s. At $TI = 270$ ms (i.e., $WM_L TI_{null}$), the signal intensities dropped significantly with increasing TE (Fig. 2D). At TI s of 275 ms and 295

ms (Figs. 2E–2F), the signal decay against TE was slower but still faster than that on the images acquired without IR preparation (Fig. 2C). Figure 3 shows bicomponent analyses of the magnitude images acquired without and with IR preparation using different TI s (ROI was defined in the center of the specimen, as illustrated in Fig. 2B). The f_S was low (7.9%) in the measurement without IR preparation (Fig. 3A), slightly higher (32.9%) at $TI = 295$ ms (Fig. 3D), and much higher (93.0%) at $TI = 270$ ms in the measurements with IR preparation (Fig. 3B), whereas the T_{2S}^* was all in the range of 150 to 400 μs (Figs. 3A–3D).

The Supporting Figure S1 (available online) shows enlarged spectra from one native (Supporting Fig. S1A) and one deuterated (Supporting Fig. S1B) WM short block. In the native specimen (Supporting Fig. S1A), the area under the water peak was much larger than that of the lipid peak and contributed $\sim 88.5\%$ of the total FID signal. In the deuterated specimen (Supporting Fig. S1B), the water peak was extremely narrow and contributed only $\sim 24.6\%$ to the total FID signal. Figure 4 shows the bicomponent fitting results of the magnitude images obtained with hard excitation pulse and no IR preparation from another deuterated WM short block that was subject to an identical deuteration procedure, revealing a f_S of $\sim 86\%$. This f_S was much higher than that in a native specimen ($\sim 7.9\%$) (Fig. 3A). This difference in f_S between the native and the deuterated specimens detected with imaging was consistent with the water-

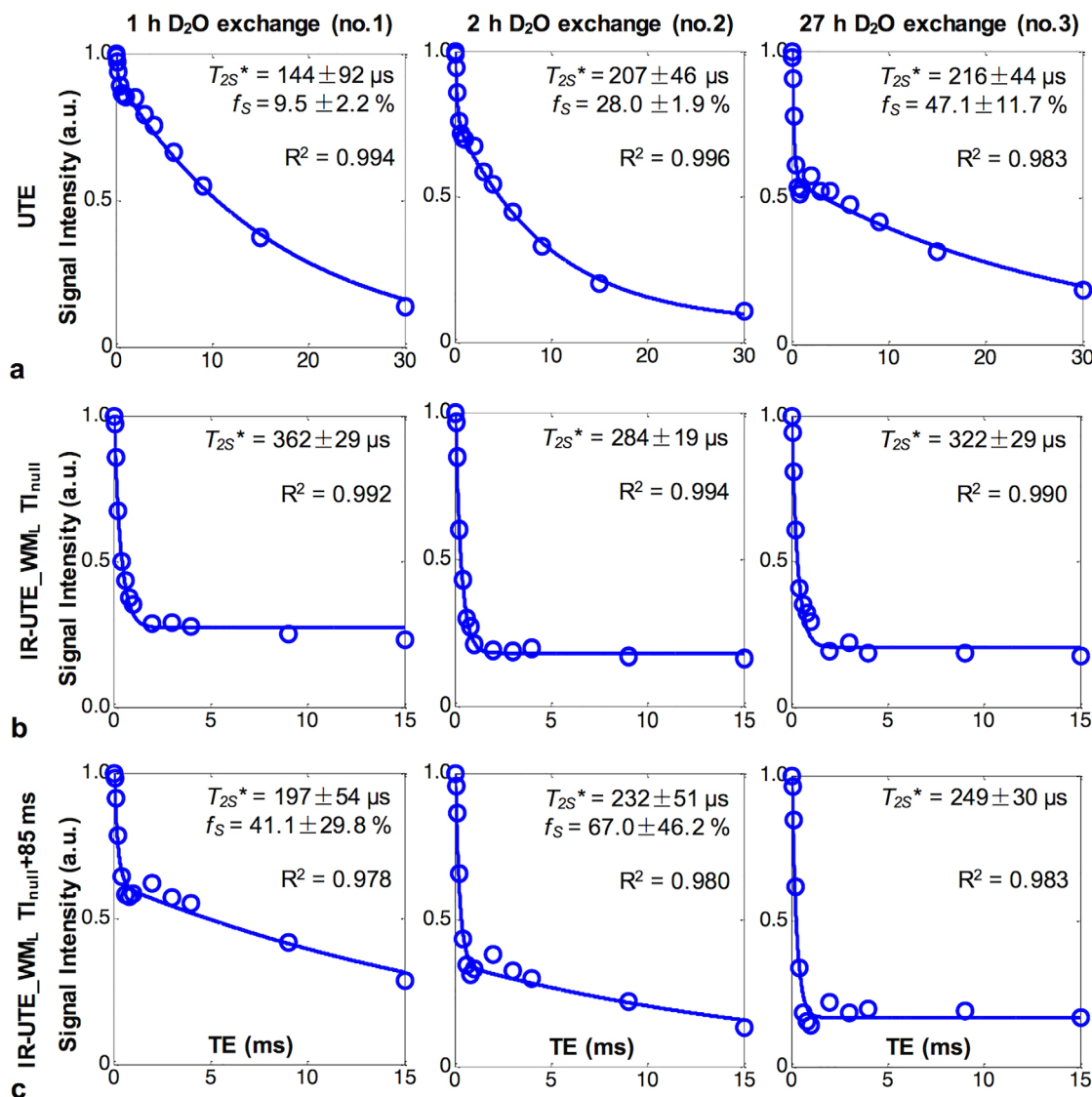


FIG. 6. T_2^* fitting curves of UTE and IR-UTE signals (all half excitation pulses) from three pure WM long segments that were subject to 1 h (left column, no. 1), 2 h (middle column, no. 2), and 27 h (right column, no. 3) exchange with D₂O, respectively. (A) The UTE sequence detected an increase of f_S from $\sim 9.5\%$ to $\sim 47.1\%$ with D₂O exchange time in specimens no. 1 to no. 3. (B) The IR-UTE images obtained at WM_L T_{1null} showed single-component T_2^* signal decay, which changed little with D₂O exchange time. (C) The IR-UTE images obtained at 85 ms longer than WM_L T_{1null} (WM_L T_{1null} + 85 ms in figure) showed bicomponent T_2^* signal decays in specimens after 1 h and 2 h D₂O exchange, and single-component T_2^* signal decay in the specimen after 27 h D₂O exchange. D₂O, deuterium oxide; f_S , ultrashort T_2 component fraction; IR, inversion recovery; T_{2S}^* , ultrashort T_2 component T_2^* , WM, white matter.

fraction reduction after D₂O exchange revealed by the FID measurements. The magnitude images (inserts in Fig. 4) from the deuterated specimen showed much faster signal decay with increasing TE than those of the native specimen (Fig. 2C), supporting unexchangeable STCs (presumably mainly myelin protons) as the major source of the UTE signals.

The Supporting Figure S2 (available online) illustrates the procedure of ROI definition in the ~ 8 -mm-thick native cerebral hemisphere slabs. Figure 5 summarizes the bicomponent T_2^* fitting results from the ~ 8 -mm-thick native cerebral hemisphere specimen (Figs. 5A–5C) shown in Supporting Figure S2 imaged using both hard and half excitation pulses, as well as the average results from three native WM short-block specimens imaged

using hard excitation pulses (Figs. 5D–5F). f_S and T_{2S}^* were identified in all specimens when measured with the UTE sequences using hard excitation pulses. However, UTE signals of the hemisphere specimen imaged using half excitation pulses showed single-component decay, and the T_2^* value was similar to T_{2L}^* in the bicomponent measurements with hard excitation pulses (Figs. 5A–5C). In the IR-UTE experiments, f_S decreased with TI when measured either with hard or half excitation pulses (Figs. 5A and 5D), and was consistently lower when measured with half pulse excitation than with hard pulse excitation at various TIs greater than WM_L T_{1null} (Fig. 5A). In all measurements, T_{2S}^* was in the range of 150 to 250 μs (Figs. 5B and 5E), and T_{2L}^* changed significantly with the increase in TI when hard pulse

Table 1
Comparison of UTE and IR-UTE Results Obtained With Half Excitation Pulses in Three Cerebral Hemisphere Slabs Before and After These Specimens Were Subjected to 27 H Four-Pass D₂O Exchange

| | Native | | | Deuterated | | |
|------------|-------------------|-------------------------|-------------------------|--------------|-------------------------|-------------------------|
| | UTE | IR-UTE (TI = 295 ms) | IR-UTE (TI = 365 ms) | UTE | IR-UTE (TI = 250 ms) | IR-UTE (TI = 380 ms) |
| T_{2S}^* | | | | | | |
| 1 | n.a. ^a | 339 ± 34 μs | 210 ± 69 μs | 239 ± 46 μs | 297 ± 21 μs | 229 ± 39 μs |
| 2 | n.a. ^a | 246 ± 28 μs | 202 ± 22 μs | 241 ± 48 μs | 245 ± 10 μs | 262 ± 35 μs |
| 3 | n.a. ^a | 215 ± 50 μs | 205 ± 64 μs | 215 ± 50 μs | 247 ± 21 μs | 262 ± 42 μs |
| f_S | | | | | | |
| 1 | n.a. ^a | ≈100% ^b | 18.0 ± 2.1% | 42.4 ± 0.4 % | ≈100% ^b | ≈100% ^b |
| 2 | n.a. ^a | ≈100% ^b | 17.5 ± 1.7% | 43.1 ± 2.2 % | ≈100% ^b | ≈100% ^b |
| 3 | n.a. ^a | ≈100% ^b | 16.0 ± 1.7% | 39.1 ± 1.3 % | ≈100% ^b | ≈100% ^b |

^aSignals on the UTE images showed single component decay with long T_2^* (22 ± 2 ms), so the T_{2S}^* and f_S readings were not available (n.a.).

^bSignals on the IR-UTE images showed single-component decay with ultrashort T_2^* .

D₂O, deuterium oxide; f_S , ultrashort T_2 component fraction; IR, inversion recovery; T_{2S}^* , ultrashort T_2 component T_2^* .

excitation was used (Figs. 5C and 5F). These results demonstrated the efficiency of the half-pulse UTE and IR-UTE sequences in measuring T_{2S}^* and detecting f_S changes in the presence of different proportions of LTCs.

Figure 6 shows T_{2S}^* and f_S measured (using half pulse excitation) from three WM long segments that were subjected to 1 h (no. 1), 2 h (no. 2), and 27 h (no. 3) D₂O exchanges, respectively. T_{2S}^* was similar across all specimens measured with either UTE sequences or IR-UTE sequences with two different TIs (85 ms apart). The UTE sequence detected an increase of f_S from ~9.5% to ~47.1% in specimens no.1 through no. 3 (Fig. 6A), consistent with progressive D₂O exchange. The IR-UTE signals of the specimen after 27 h D₂O exchange (no. 3) could be characterized using single-component fitting at both TIs used, suggesting that f_S was less dependent on TI as the D₂O exchange progressed.

Table 1 shows T_{2S}^* and f_S measured (using half pulse excitation) from three hemisphere slabs before and after 27 h exchange with D₂O. Before exchange with D₂O, the UTE signals showed single-component decay with a long T_2^* (~24 ms), and f_S and T_{2S}^* values could not be obtained. Meanwhile, the IR-UTE signals could be characterized through single-component T_2^* fitting at TI = 295 ms (i.e., WM_L TI_{null}) or through bicomponent T_2^* fitting at TI = 365 ms, with f_S values of less than 20% in all specimens. After exchange with D₂O, the UTE signals contained a f_S of ~40% and the IR-UTE signals showed single-component decay at both TIs used (i.e., TIs = 250 ms and 380 ms). T_{2S}^* was in the range of 200 to 400 μs either before or after exchange in all specimens. These results further support that protons that were unexchangeable with D₂O can be measured by UTE and IR-UTE sequences when used with half excitation pulses.

DISCUSSION

The present study used a bicomponent T_2^* fitting model as a simplified means to quantify f_S and T_{2S}^* in WM. In UTE images obtained with hard pulse excitation, f_S was found to be ~4% to 8% in native specimens and up to 86% in deuterated specimens. In IR-UTE images obtained with either hard or half pulse excitation, f_S was

close to 100% at WM_L TI_{null} and decreased significantly with increasing TI in native specimens but not in deuterated specimens. T_{2S}^* was found to be 150 to 400 μs in both native and deuterated specimens imaged using either hard pulse or half pulse excitations, and was consistent with previously reported values in myelin extract and nerve tissue (14,22).

Results Obtained With Hard or Half Excitation Pulses

This study first tested the UTE and IR-UTE sequences with hard excitation pulses in pure WM short blocks using a 5 mm-diameter solenoid coil that produces high SNR. The results showed that the f_S was strongly dependent on the choice of TI, whereas T_{2S}^* was not. When TI was increased by 5 ms and then by 25 ms from WM_L TI_{null}, f_S decreased from ~100% to ~62% and then to ~34%, respectively. Then, the sequences were used to image a native cerebral hemisphere slab using both hard and half excitation pulses. The UTE sequence failed to identify the WM_S when used with half excitation pulses, and the IR-UTE sequence detected consistently lower f_S values using half excitation pulses than hard excitation pulses over a range of TIs that were offset from WM_L TI_{null}. These results are consistent with the expectation that the half excitation pulses had lower efficiency than hard excitation pulses in detecting STCs. As compared with the half excitation pulses, the hard excitation pulses have shorter durations (32 μs vs. 472 μs), thus broader bandwidth (8.2 kHz vs. 2.7 kHz) and higher efficiency in exciting ultrashort T_2 components (20,23,25). However, with TI set at WM_L TI_{null}, T_{2S}^* could be measured through single-component fitting of the multi-TE IR-UTE signals obtained using half excitation pulses, with the results similar to those obtained using hard excitation pulses. Furthermore, the IR-UTE sequences used with either hard or half excitation pulses were able to provide stable T_{2S}^* values and detect the differences in f_S when varying TIs were used. These results support the view that it is possible to use the IR-UTE sequences with half excitation pulses to detect STCs using clinical whole-body MR scanners.

Comparison of T_{2S}^* and f_S in Native and Deuterated Specimens

This study included three D₂O exchange experiments. First, two WM mini-blocks were subjected to an identical 8 h five-pass D₂O exchange procedure and imaged using hard excitation pulses. After exchange, the specimens showed a very narrow HDO peak in the FID spectrum at 11.7T, and an f_S as high as ~86% on UTE images at 3T versus ~7.9% in the native specimen. In the TE range of 10 μ s to 4 ms, the UTE images of the deuterated specimen showed marked signal intensity decay with increasing TE, in contrast to the barely observable changes in the native specimen. This experiment confirmed significant water signal loss in the deuterated specimen, and proved that UTE sequences used with hard excitation pulses are sensitive to proportional water proton and myelin proton content changes in biological tissue. Second, three pure WM long segments were subjected to different durations of D₂O exchange and imaged using half excitation pulses. When the specimens were imaged using UTE sequences, f_S was observed to increase from ~9.5% (1 h, one-pass exchange) to ~47.1% (27 h, four-pass exchange). When the specimens were imaged using IR-UTE sequences, f_S was shown to be less affected by the choice of TI as the D₂O exchange duration increased. This experiment demonstrated that UTE and IR-UTE sequences used with half excitation pulses are also sensitive to proportional water proton and myelin proton content changes in biological tissue. Lastly, three cerebral hemisphere slabs were imaged using half excitation pulses both before and after a 27 h four-pass D₂O exchange. Results obtained from these specimens further confirmed an increase in f_S after D₂O exchange (f_S = ~39%–42% vs. unmeasurable) when measured using UTE sequences. In all three experiments, when the UTE or IR-UTE sequences were used with either hard or half excitation pulses, the T_{2S}^* values were consistently in the range of 150 to 400 μ s both before and after exchange with D₂O. Furthermore, these T_{2S}^* values were comparable with those obtained using the same protocols from myelin powder as well as a myelin paste in D₂O (22). These results jointly suggest that the ultrashort T_2^* signals survived D₂O exchange and provide evidence to support that 1) myelin, presumably the nonexchangeable methylene groups (14), is the major source of the ultrashort T_2^* signals seen in WM on IR-UTE images; and 2) half-pulse IR-UTE sequences are sensitive to myelin concentration changes and therefore could be used for direct quantification of myelin loss.

Because myelin has a tightly organized, closely packed, highly stable structure with a hydrophobic core (28), complete replacement of water protons in nervous tissue with deuterons may be difficult, and the efficiency may depend on the form and type of tissue the myelin is in. For example, Horch et al. detected a loss of ~95% of the LTCs in a frog sciatic nerve (peripheral nerve), but only ~68% in a rat optic nerve (cranial nerve) after both nerves were incubated in D₂O buffer for 2 h (14). This might be associated with the structural and chemical differences of myelin tissue in the two nerves (29). Even after a rat optic nerve was immersed in D₂O buffer for 10 days, only a loss of ~82% of LTCs was observed (14).

All the specimens used in the present study were much larger in size than the frog sciatic or rat optic nerves (~1 mm or smaller in diameter) used in the Horch et al.'s study (14). This might explain why our UTE experiments only detected an f_S of ~86% (instead of ~100%) in a WM short block (small specimen) after 8 h, five-pass D₂O exchange, and ~39% to 47% in the larger specimens (one WM long segment and three cerebral hemisphere slabs) after 27 h, four-pass D₂O exchange. The relatively lower f_S in the larger specimens relative to that in the small specimen might be due to difference in the efficiency of D₂O exchange, the lower efficiency of half pulse excitation relative to hard pulse excitation, and the lower SNR obtained with the 76-mm surface coil compared to the 5 mm solenoid coil.

Comparison of Magnetization Transfer and IR-UTE Measurements of Myelin Tissue

The restricted proton pool (STCs) in white matter include not only protons in myelin lipids but also those in proteins and other semisolid membrane components. According to the literature (13,14) and our own results, the ultrashort T_2^* signals (T_2^* , ~300 μ s) primarily arise from protons in methyl (–CH₃) and methylene (–CH₂) groups of phospholipids in myelin tissue. If the observed short T_2^* signals were mainly from proteins, they would not survive D₂O exchange because protons in amino (–NH₂) and carboxyl (–COOH) groups in the majority of proteins could be exchanged with deuterons in D₂O. Protons in proteolipid proteins, which are highly hydrophobic, may survive D₂O exchange, but the proteolipid proteins-to-lipid ratio in brain myelin is about 1:9 (30). Therefore, the contribution from these protons, if any, would be very small. Magnetization transfer (MT) is another MR contrast mechanism that has been used to probe the restricted proton pool by measuring the magnetization exchange between the restricted proton pool and the free proton pool (10,31,32). Carboxyl (–COOH) groups on cholesterol and galactocerebrosides are thought to be the major interaction sites between the restricted pool and the free pool for magnetization exchange (33–35). Therefore, MT contrast and the measured contrast in this study provide different aspects of information of the restricted proton pool. Furthermore, MT ratio derived from MT imaging is an indirect measure, whereas the IR-UTE sequence provides a direct measure of STCs. Therefore, we believe the measured contrast is more specific to myelin lipid protons than MT ratio.

Limitations

The WM_L T_{1null} was estimated in this study using the same IR-UTE sequence as that used for T_{2S}^* measurement, with the intention of eliminating sequence-dependent T_1 measurement inaccuracy (36). However, the T_1 signals of LTCs were modeled using a single-component fitting model, and the T_2^* signals were fitted using the magnitude images for simplicity. It has been reported that there are two or more T_1 relaxation pools in brain tissue that are associated with distinctive T_2 relaxation rates (37,38) and these might have different T_{1s} . Therefore,

our approach might induce insufficient nulling of LTC signals, as suggested by the observation that the value of f_S was not 100% in native WM in IR-UTE experiments at $WM_L TI_{null}$ (Fig. 2E). Fitting the signal in complex images would provide more accurate estimation of f_S . In addition, more advanced inversion recovery UTE sequences are currently under investigation by our team (39) and another group (40) to simultaneously suppress long T_2 water signals with a broad range of T_1 s. Second, our f_S values were relatively small compared with the known myelin tissue concentration in the wet mass of WM (41,42). This might be due to insufficient nulling of LTCs. In addition, one previous NMR spectroscopy experiment at 9.4T revealed multiple T_2^* components in purified bovine myelin extract (suspended in D_2O), with 26.4% of the total signal having an effective lifetime of $< 25 \mu s$, 51.8% of $< 0.1 ms$, and 91.6% of $< 1 ms$ (at $20^\circ C$) (21). The supershort T_2 components (T_2 , 0.01–0.1 ms) are probably not accessible by our UTE/IR-UTE imaging experiments at 3T. Third, a simplified bi-component model was used in this study to fit the T_2^* signals in the magnitude IR-UTE images. The T_{2L}^* has limited biophysical meaning because it is associated with multiple water pools. Multicomponent models might be desirable in order to fully capture the tissue relaxation properties. However, such analysis can be very challenging and is prone to errors; thus, it needs further investigation. Fourth, plain D_2O was used in this study to replace H_2O in the specimens. Ideally D_2O buffer should be used to mimic physiological osmotic pressure and pH effects. Nonetheless, the T_{2S}^* values before and after D_2O exchange were relatively consistent in our study, suggesting that the T_{2S}^* was not significantly affected by incubation in plain D_2O , possibly because the methylene groups that are known to form hydrophobic nonpolar hydrocarbon chains (28) were not interchangeable with or inaccessible by D_2O (14). Fifth, cross-relaxation between macromolecules and water was not considered in this study. Such cross-relaxation can produce apparent shortening of T_1 and T_2 (31,43), but its effects on ultrashort T_2^* values are not fully understood. However, it is unlikely to have significantly affected the ultrashort T_2^* signals measured in this study. In this study, the $WM_L TI_{null}$ was directly determined via fitting the IR-UTE images obtained with different TIs. Cross-relaxation-induced T_1 -shortening would only result in a shorter estimated $WM_L TI_{null}$. Meanwhile, the ultrashort T_2^* values were largely consistent in specimens before and after different durations of D_2O exchange, further suggesting our measurements were unlikely significantly contaminated by cross-relaxation between the restricted proton pool and the free water pool. This might be further confirmed through comparing the T_2^* fitting results obtained with UTE experiments with or without magnetization transfer preparation. Lastly, the 2D IR-UTE sequences typically employ slice-selective half excitation pulses for in vivo studies. Eddy currents associated with the slice-selective gradients may lead to out-of-slice signal contamination (20,44), thus affecting T_2^* analysis. This error can be reduced by measuring the slice-selective gradients, adding precompensation gradients, and/or using the measured readout gradients for re-gridding (45). In this study, we used nonselective gradients to minimize

eddy currents and speed up data acquisition. The use of nonselective pulses is valid as the focus of this paper is to further demonstrate that myelin protons are directly detectable with 2D IR-UTE sequences on a clinical MR scanner. Further work is needed to increase the robustness of this sequence by using advanced gradient calibration and image reconstruction techniques.

CONCLUSION

The f_S values were significantly affected by the TIs used in IR-UTE sequences with either hard or half excitation pulses in native specimens but not in heavily deuterated specimens. T_{2S}^* was in the range of 150 to 400 μs in all measurements made with either hard or half-pulse excitation UTE and IR-UTE sequences. The major source of the ultrashort T_2^* signals seen in WM on IR-UTE images is likely to be myelin protons, presumably methylene groups. Half-pulse IR-UTE sequences have the potential for direct qualitative and quantitative myelin imaging.

REFERENCES

1. Laule C, Vavasour IM, Kolind SH, Li DK, Traboulsee TL, Moore GR, MacKay AL. Magnetic resonance imaging of myelin. *Neurotherapeutics* 2007;4:460–484.
2. Alexander AL, Hurley SA, Samsonov AA, Adluru N, Hosseinbor AP, Mossahebi P, Tromp do PM, Zakszewski E, Field AS. Characterization of cerebral white matter properties using quantitative magnetic resonance imaging stains. *Brain Connect* 2011;1:423–446.
3. Montagne A, Barnes SR, Sweeney MD, et al. Blood-brain barrier breakdown in the aging human hippocampus. *Neuron* 2015;85:296–302.
4. Wardlaw JM, Farrall A, Armitage PA, Carpenter T, Chappell F, Doubal F, Chowdhury D, Cvro V, Dennis MS. Changes in background blood-brain barrier integrity between lacunar and cortical ischemic stroke subtypes. *Stroke* 2008;39:1327–1332.
5. Starr JM, Farrall AJ, Armitage P, McGurn B, Wardlaw J. Blood-brain barrier permeability in Alzheimer's disease: a case-control MRI study. *Psychiatry Res* 2009;171:232–241.
6. Assaf Y, Pasternak O. Diffusion tensor imaging (DTI)-based white matter mapping in brain research: a review. *J Mol Neurosci* 2008;34:51–61.
7. Cao P, Hyder F, Zhou IY, Zhang JW, Xie VB, Tsang A, Wu EX. Simultaneous spin-echo and gradient-echo BOLD measurements by dynamic MRS. *NMR Biomed* 2017. doi: 10.1002/nbm.3745.
8. Le Bihan D. Diffusion, confusion and functional MRI. *Neuroimage* 2012;62:1131–1136.
9. Mollink J, Kleinmijhuis M, Cappellen van Walsum AV, et al. Evaluating fibre orientation dispersion in white matter: Comparison of diffusion MRI, histology and polarized light imaging. *Neuroimage* 2017; 157:561–574.
10. Naumova AV, Akulov AE, Khodanovich MY, Yarnykh VL. High-resolution three-dimensional macromolecular proton fraction mapping for quantitative neuroanatomical imaging of the rodent brain in ultrahigh magnetic fields. *Neuroimage* 2017;147:985–993.
11. Nguyen TD, Spincemaille P, Gauthier SA, Wang Y. Rapid whole brain myelin water content mapping without an external water standard at 1.5T. *Magn Reson Imaging* 2017;39:82–88.
12. Alonso-Ortiz E, Levesque IR, Pike GB. Multi-gradient-echo myelin water fraction imaging: comparison to the multi-echo-spin-echo technique. *Magn Reson Med* 2018;79:1439–1446.
13. Ramani A, Aliev AE, Barker GJ, Tofts PS. Another approach to protons with constricted mobility in white matter: pilot studies using wide-line and high-resolution NMR spectroscopy. *Magn Reson Imaging* 2003;21:1039–1043.
14. Horch RA, Gore JC, Does MD. Origins of the ultrashort-T2 1H NMR signals in myelinated nerve: a direct measure of myelin content? *Magn Reson Med* 2011;66:24–31.
15. Mathews PM, Roncaroli F, Waldman A, Sormani MP, De Stefano N, Giovannoni G, Reynolds R. A practical review of the neuropathology and neuroimaging of multiple sclerosis. *Pract Neurol* 2016;16:279–287.

16. Wang Y, Sun P, Wang Q, Trinkaus K, Schmidt RE, Naismith RT, Cross AH, Song SK. Differentiation and quantification of inflammation, demyelination and axon injury or loss in multiple sclerosis. *Brain* 2015;138:1223–1238.
17. Robson MD, Gatehouse PD, Bydder M, Bydder GM. Magnetic resonance: an introduction to ultrashort TE (UTE) imaging. *J Comput Assist Tomogr* 2003;27:825–846.
18. Waldman A, Rees JH, Brock CS, Robson MD, Gatehouse PD, Bydder GM. MRI of the brain with ultra-short echo-time pulse sequences. *Neuroradiology* 2003;45:887–892.
19. Du J, Ma G, Li S, Carl M, Szevenyeni NM, Vandenberg S, Corey-Bloom J, Bydder GM. Ultrashort echo time (UTE) magnetic resonance imaging of the short T2 components in white matter of the brain using a clinical 3T scanner. *Neuroimage* 2014;87:32–41.
20. Larson PE, Gurney PT, Nayak K, Gold GE, Pauly JM, Nishimura DG. Designing long-T2 suppression pulses for ultrashort echo time imaging. *Magn Reson Med* 2006;56:94–103.
21. Wilhelm MJ, Ong HH, Wehrli SL, Li C, Tsai PH, Hackney DB, Wehrli FW. Direct magnetic resonance detection of myelin and prospects for quantitative imaging of myelin density. *Proc Natl Acad Sci U S A* 2012;109:9605–9610.
22. Sheth V, Shao H, Chen J, Vandenberg S, Corey-Bloom J, Bydder GM, Du J. Magnetic resonance imaging of myelin using ultrashort Echo time (UTE) pulse sequences: phantom, specimen, volunteer and multiple sclerosis patient studies. *Neuroimage* 2016;136:37–44.
23. Larson PE, Conolly SM, Pauly JM, Nishimura DG. Using adiabatic inversion pulses for long-T2 suppression in ultrashort echo time (UTE) imaging. *Magn Reson Med* 2007;58:952–961.
24. Muller S, Seelig J. In vivo NMR imaging of deuterium. *J Magn Reson* 1987;72:456–466.
25. Carl M, Bydder M, Du J, Takahashi A, Han E. Optimization of RF excitation to maximize signal and T2 contrast of tissues with rapid transverse relaxation. *Magn Reson Med* 2010;64:481–490.
26. Li S, Ma L, Chang EY, Shao H, Chen J, Chung CB, Bydder GM, Du J. Effects of inversion time on inversion recovery prepared ultrashort echo time (IR-UTE) imaging of bound and pore water in cortical bone. *NMR Biomed* 2015;28:70–78.
27. Fan SJ, Ma Y, Chang EY, Bydder GM, Du J. Inversion recovery ultrashort echo time imaging of ultrashort T2 tissue components in ovine brain at 3T: a sequential D2O exchange study. *NMR Biomed* 2017. doi: 10.1002/nbm.3767.
28. O'Brien JS. Stability of the myelin membrane. *Science* 1965;147:1099–1107.
29. Finean JB, Hawthorne JN, Patterson JD. Structural and chemical differences between optic and sciatic nerve myelins. *J Neurochem* 1957;1:256–259.
30. Kalwy SA, Smith R. Mechanisms of myelin basic protein and proteolipid protein targeting in oligodendrocytes (review). *Mol Membr Biol* 1994;11:67–78.
31. Wolff SD, Balaban RS. Magnetization transfer contrast (MTC) and tissue water proton relaxation in vivo. *Magn Reson Med* 1989;10:135–144.
32. Henkelman RM, Stanisz GJ, Graham SJ. Magnetization transfer in MRI: a review. *NMR Biomed* 2001;14:57–64.
33. Ceckler TL, Wolff SD, Yip V, Simon SA, Balaban RS. Dynamic and chemical factors affecting water proton relaxation by macromolecules. *J Magn Reson* 1992;98:637–645.
34. Koenig SH, Brown RD, Spiller M, Lundbom N. Relaxometry of brain: why white matter appears bright in MRI. *Magnet Reson Med* 1990;14:482–495.
35. Kucharczyk W, Macdonald PM, Stanisz GJ, Henkelman RM. Relaxivity and magnetization-transfer of white-matter lipids at MR-imaging: importance of cerebroside and pH. *Radiology* 1994;192:521–529.
36. Stikov N, Boudreau M, Levesque IR, Tardif CL, Barral JK, Pike GB. On the accuracy of T1 mapping: searching for common ground. *Magn Reson Med* 2015;73:514–522.
37. Deoni SC, Rutt BK, Arun T, Pierpaoli C, Jones DK. Gleaning multi-component T1 and T2 information from steady-state imaging data. *Magn Reson Med* 2008;60:1372–1387.
38. Does MD, Gore JC. Compartmental study of T(1) and T(2) in rat brain and trigeminal nerve in vivo. *Magn Reson Med* 2002;47:274–283.
39. Ma YJ, Zhu Y, Lu X, Carl M, Chang EY, Du J. Short T2 imaging using a 3D double adiabatic inversion recovery prepared ultrashort echo time cones (3D DIR-UTE-cones) sequence. *Magn Reson Med* 2018;79:2555–2563.
40. Harkins K US, Nyman J, Does M. Robust pore water suppression in cortical bone with multiple adiabatic inversion recovery. In Proceedings of the 25th Annual Meeting of ISMRM, Honolulu, Hawaii, USA, 2017. p. 1588.
41. Malone MJ, Szoke MC. Neurochemical changes in white matter. Aged human brain and Alzheimer's disease. *Arch Neurol* 1985;42:1063–1066.
42. van der Knaap M, Valk J. Myelin and white matter. In: Heilmann U, Mennecke-Buhler D, eds. *Magnetic Resonance of Myelination and Myelin Disorders*. Berlin, Heidelberg, Germany: Springer; 2005: 1–19.
43. Gochberg DF, Gore JC. Quantitative imaging of magnetization transfer using an inversion recovery sequence. *Magn Reson Med* 2003;49:501–505.
44. Wansapura JP, Daniel BL, Pauly J, Butts K. Temperature mapping of frozen tissue using eddy current compensated half excitation RF pulses. *Magn Reson Med* 2001;46:985–992.
45. Lu A, Daniel BL, Pauly JM, Pauly KB. Improved slice selection for R2* mapping during cryoablation with eddy current compensation. *J Magn Reson Imaging* 2008;28:190–198.

SUPPORTING INFORMATION

Additional supporting information may be found in the online version of this article.

Fig. S1. Spectra from two white-matter (WM) short blocks examined either in the native condition or after 27 h immersion in deuterium oxide (D₂O). (A) Spectrum from one WM short block examined in the native condition. The integrated area under the water peak: the total area = 1:1.13, suggesting a ~88.5% contribution from water to the total signal. (B) Spectrum from one WM short block examined after 27 h immersion in D₂O (four changes of D₂O with intervals of 1 h, 1 h, 2 h, and 23 h). The integrated area under the water peak: the total area = 1:4.07, suggesting a ~24.6% contribution from water to the total signal.

Fig. S2. Illustration of the procedure for defining the region of interest (ROI) in white matter for myelin proton T₂ quantification in cerebral hemisphere slabs. The images were from the ~8 mm thick cerebral hemisphere slab. Yellow boxes show the final ROI. (A–H) Eight consecutive T₂-weighted fast spin echo (FSE) images (TR/TE = 3000 ms/40 ms, slice thickness = 1 mm, and no slice gap). (I) The maximum intensity projection (MIP) of (A) to (H). (J) The IR-UTE image (TR/TI/TE = 1000/300/2.2 ms, half pulse excitation, slice-selective gradient turned off) showing similar contrast between white matter (low signal) and grey matter (high signal) as (I). The ROI was first manually drawn on the IR-UTE image (J), copied to the multi-slice T₂-weighted FSE images (A–H) and then refined to exclude any gray matter contamination.